Local Electronic Structure of MgB_2 by X-Ray Raman Scattering at the Boron K Edge

A. Mattila,[1,*] J. A. Soininen,[1] S. Galambosi,[1] S. Huotari,[2] G. Vankó,[2] N. D. Zhigadlo,[3] J. Karpinski,[3] and K. Hämäläinen[1]

[1]*Division of X-Ray Physics, Department of Physical Sciences, POB 64, 00014 University of Helsinki, Finland*

[2]*European Synchrotron Radiation Facility, BP 220, 38043 Grenoble, France*

[3]*Solid State Physics Laboratory, ETH, CH-8093 Zürich, Switzerland*

(Received 27 January 2005; published 22 June 2005)

We have investigated the electronic structure of MgB_2 using x-ray Raman scattering at the boron K edge in a single crystal sample. Using both the direction and the magnitude dependence of the momentum transfer we can identify the spatial orientation of empty electronic states with different symmetries. The local symmetry-resolved electronic structure of MgB_2 is analyzed using two independent first-principles computational approaches. We show that near the Fermi level the density of s symmetry states is vanishingly small. We also identify and separate the contributions from boron $p_{xy}(\sigma)$ and $p_z(\pi)$ states, which play an important role in determining the superconducting properties of MgB_2.

DOI: 10.1103/PhysRevLett.94.247003 PACS numbers: 74.25.Jb, 71.15.−m, 74.70.Ad, 78.70.Ck

The discovery of a relatively high critical temperature $T_C \approx 39$ K of superconductivity in MgB_2 [1] has sparked off a considerable number of experimental and theoretical investigations of the electronic structure and the mechanism behind the high transition temperature [2]. Based on these studies MgB_2 is now understood to be a phonon-mediated Eliashberg superconductor with two superconducting energy gaps [3–9] originating from the boron p σ and π bands due to different electron-phonon coupling strengths. The σ band holes, with a large density of states near the Fermi level, drive the superconductivity through a strong coupling to B-B bond-stretching phonon modes [10–12]. This picture is consistent with the destruction of the superconductivity with the filling of the σ band holes by Al substitution [13].

X-ray Raman scattering (XRS) [14] is well suited to probe the electronic structure of MgB_2, making possible studies of spatial orientation of empty electronic states with different symmetries. The anisotropies of the empty electronic states in MgB_2 have been previously investigated using electron energy loss spectroscopy (EELS) [15–17] and x-ray absorption spectroscopy (XAS) [18,19] at the boron K edge, in order to separate the σ and π band states. To our knowledge, however, no experiments probing also the empty s symmetry states of boron have been performed on MgB_2, even though the momentum transfer dependence of the EELS cross section [20] would, in principle, permit such studies.

In this study we have used XRS at the boron K edge in single crystal MgB_2 to probe the empty boron electronic states, especially the interesting σ and π bands. As we use hard x-rays we probe the bulk of the sample, which is an advantage considering the hygroscopic nature of MgB_2 crystals [21]. We find an excellent agreement between the experimental data and our calculations of the XRS cross section and the electronic structure of MgB_2. Using the momentum transfer dependence of the XRS we can separate the contributions from both the boron σ and π bands, and furthermore, probe also the empty states with s symmetry.

The double-differential cross section for XRS is given by

$$\frac{d^2\sigma}{d\Omega d\omega} = \left(\frac{d\sigma}{d\Omega}\right)_{\mathrm{Th}} \sum_f \left| \left\langle f \left| \sum_j e^{i\vec{q}\cdot\vec{r}_j} \right| i \right\rangle \right|^2 \delta(E_f - E_i - \omega),$$

where $(d\sigma/d\Omega)_{\mathrm{Th}}$ is the Thomson scattering cross section and $\vec{q}$ and ω are the momentum and energy transfers from the photons to the electrons at positions r_j. In the expression, $|i\rangle$ and $|f\rangle$ are the initial and final electron states with energies E_i and E_f, respectively. The exponential term in the matrix element can be expanded as $\exp(i\vec{q}\cdot\vec{r}) = 1 + i\vec{q}\cdot\vec{r} + (i\vec{q}\cdot\vec{r})^2/2 + \cdots$. The first term in the expansion does not contribute as the initial and final states are orthogonal. At low momentum transfer values (when $qa \ll 1$, where a is the core electron orbital radius) the second term, i.e., dipole allowed transitions, dominates the spectrum. At this limit the XRS cross section has a clear similarity to the cross section for XAS, with the momentum transfer vector playing the role of the polarization vector in XAS. In fact, the two cross sections can be shown to be proportional within the dipole limit [14], as confirmed also by various experimental studies [22,23], allowing the measurement of low energy absorption edges of light elements using hard x-rays [24]. For high momentum transfers ($qa > 1$) monopolar and quadrupolar transitions, rising from the third term in the expansion of $e^{i\vec{q}\cdot\vec{r}}$, may start to contribute significantly as the intensity of these features scales as q^2 relative to dipolar excitations. By observing the q-dependent evolution of the spectral features, it is possible to try to separate these different excitation channels, as was demonstrated in Ref. [25], for example.

A single crystal MgB_2 sample for the experiment was grown using a high pressure anvil technique [26]. The resulting platelike sample was characterized using magne-

tization measurements and was found to undergo a superconducting transition at 38.7 K. The quality and orientation of the sample was verified using the x-ray Laue technique. MgB_2 crystallizes into the AlB_2 structure [27] with alternating hexagonal Mg and graphitelike B layers running in the ab plane with the c axis perpendicular to these. The crystal size was roughly 500 μm $\times$ 300 μm, with a thickness of about 100 μm and with the [001] direction (the c axis) perpendicular to the larger face. The experiment was performed at the beam line ID16 at the European Synchrotron Radiation Facility. Incident radiation was monochromatized using a Si(111) double-crystal monochromator and the scattered photons were analyzed in energy using a spherically bent Si crystal with a bending radius of 1 m, operating in a horizontal Rowland circle scattering geometry. The sample was at room temperature and kept under He atmosphere during the experiment. We observed no signs of sample degradation either by visual inspection of the sample or as changes between XRS spectra measured at the start and at the end of the experiment.

The XRS spectra were measured for $q = 2.1$ Å^{-1}, 4.0 Å^{-1}, and 9.7 Å^{-1}, with $\vec{q} \parallel [100]$ (the a axis along the boron planes) and $\vec{q} \parallel [001]$ (the c axis perpendicular to the boron planes). The energy transfer scans were performed using the inverse energy scan technique [28,29], where the scattered photons are analyzed at a fixed energy and the energy transfer is controlled by tuning the incident photon energy. For $q = 2.1$ Å^{-1} and 4.0 Å^{-1} the scattered photons were analyzed using the Si(444) reflection with a fixed energy of 7908.3 eV and for 9.7 Å^{-1} using the Si(555) reflection with a fixed energy of 9885.4 eV eV. The overall energy resolution for $q = 2.1$ Å^{-1} and 4.0 Å^{-1} was 1.0 eV and for $q = 9.7$ Å^{-1} 1.4 eV, as estimated from the full width at half maximum of the quasielastic line.

The spectra were finally corrected for the inelastic scattering from the valence and Mg $2s$ and $2p$ electrons by approximating the smooth inelastic background with a second degree polynomial. Well above the threshold the slope of the corrected spectra has some sensitivity to the exact parameters of the correction. For the first 40 eV above the threshold, however, the spectra are largely unaffected by the specifics of the background removal. Hence, our analysis of the near edge structures does not depend on the details of the background removal.

To analyze the spectra in more detail we performed first-principles calculations of the XRS cross section using a scheme based on the Bethe-Salpeter equation (BSE) [30,31]. We also used the real space multiple scattering (MS) code FEFF8 [32] to calculate the site and symmetry projected electronic density of states (ℓDOS) and the polarized boron K-edge XAS [33]. The BSE scheme uses the $\vec{q}$-dependent matrix elements for the calculation of the XRS cross section. The MS code, however, does not currently include the matrix elements for XRS and the calculated absorption spectra can be compared directly only with the low momentum transfer spectra, as with $q = 2.1$ Å^{-1} the parameter $qa < 1$ and the spectra are well within the dipole transition region.

The experimental spectra and the BSE scheme calculation for $\vec{q} \parallel [100]$ and $\vec{q} \parallel [001]$ are shown in Figs. 1(a) and 1(b), respectively. In Fig. 1 we also show the MS calculation of the absorption spectra together with a calculation in which the core hole is not included in the final state. The calculated spectra are convoluted with the corresponding experimental energy resolution and shifted in energy to align with the experimental data. The intensities of the experimental XRS spectra and of the spectra calculated using the BSE scheme are scaled to the value of peak C for $\vec{q} \parallel [100]$ and peak D′ for $\vec{q} \parallel [001]$ to facilitate a detailed discussion.

The experiment reveals a clear difference between $\vec{q} \parallel [100]$ and $\vec{q} \parallel [001]$. A well separated peak A before the leading edge is observed in Fig. 1(a), whereas in Fig. 1(b) a sharp absorption threshold is followed by broad features A′ and B′ with nearly equal intensities at low momentum transfer. At both directions the spectra show systematic changes as the magnitude of the momentum transfer is tuned. For $\vec{q} \parallel [100]$ the peak A loses spectral weight, whereas the feature B gains in intensity, and the position of the peak maximum shifts to smaller energy transfer by roughly 0.5 eV when q increases from

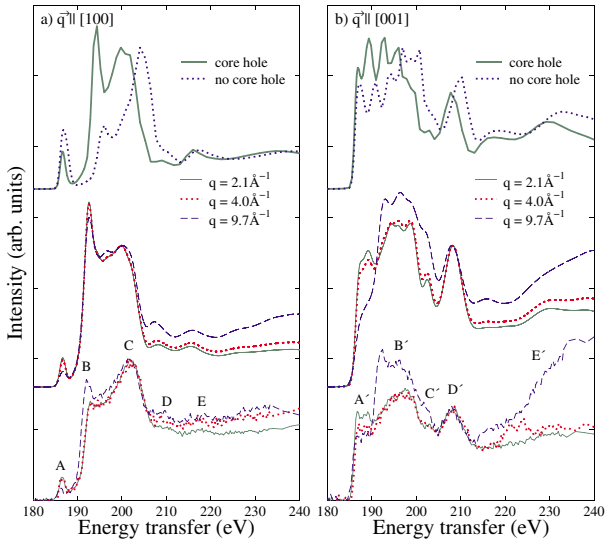

FIG. 1 (color online). (a) The experimental (lower part) and BSE scheme calculation of (middle part) boron K-edge XRS spectra measured with $\vec{q} \parallel [100]$. (b) is the same as (a) except $\vec{q} \parallel [001]$. The q values for the experimental and for the spectra calculated using the BSE scheme are indicated in the figure. The letters A–E and A′–E′ refer to identifiable features in the experimental spectra and are discussed in the text. The upper parts show the absorption spectra calculated using the MS approach with (solid line) and without (dotted line) the core hole.

2.1 Å^{-1} to 9.7 Å^{-1}. For $\vec{q} \parallel [001]$ we also observe the feature A′ right above the threshold to lose spectral weight, whereas the broad features B′ and C′ gain significantly in intensity as q increases. In both directions the measurements show a gain in intensity well above the threshold with increasing q, although, as previously noted, the exact slope of the spectra high above the threshold depends to some extent on the background subtraction.

The XRS spectra calculated using the BSE scheme show a very good agreement with the experiment in both directions, considering both the agreement between individual spectra and the overall evolution of the spectral features as a function of q. Also, the absorption spectra calculated with the MS code are well in agreement with the experimental results for $q = 2.1$ Å^{-1}. For $\vec{q} \parallel [100]$ all the peaks A through E are present in both calculations although the intensity of peak B is overestimated and BSE calculation shows diminishing intensity with increasing q for this feature. For $\vec{q} \parallel [001]$ direction the overall agreement is also very good even though MS calculation shows extra structure for features A′ and B′. It is quite curious to note that both calculations with different approaches overestimate for $\vec{q} \parallel [100]$ the intensity of the peak B by almost equal amounts, although the correspondence with the experiment before and after this narrow region is very good.

The decomposition of the XRS spectra calculated using the BSE scheme into contributions from excitations to s and p symmetry final states reveals for $q = 2.1$ Å^{-1} only a few percent contribution from s symmetry final states. This further confirms that for the lowest momentum transfer value the spectra are dominated by dipole allowed transitions. At higher momentum transfers, monopole transitions start to contribute significantly. In Figs. 2(a) and 2(b) we show the decomposition of the XRS spectra calculated using the BSE scheme for both orientations of $\vec{q}$ for $q = 9.7$ Å^{-1}. In both directions above 190 eV energy transfer monopolar transitions contribute significantly to the overall spectral intensity. The increased contribution from s type final states clearly explains most of the changes in the experimental spectra in Figs. 1(a) and 1(b) with increasing q. The dipole part has a minor contribution to these changes with a small increase in intensity at energy transfers of roughly 20 eV and above over the threshold. The decrease of the features A and A′ intensity in Figs. 1(a) and 1(b) with increasing q is explained by the almost zero contribution from s symmetry final states right above the threshold. We also note that the contributions from excitations to d type states are negligible at the energy range shown in Fig. 2 even at high q and are not shown in the figure.

For $\vec{q} \parallel [100]$ the dipole transitions reach the p_{xy} states, whereas for $\vec{q} \parallel [001]$ the p_z states are probed. For Fig. 1(a) this indicates that the peak A is formed by transitions into p_{xy} states whereas the broad feature A′ in Fig. 1(b) is stemming from the p_z final states. Within the band structure approach the two-dimensional σ band residing in the boron planes is derived from the p_{xy} states, whereas the π band derives from the p_z states oriented perpendicular to the boron planes.

Since the contributions from the p symmetry final states to the XRS cross section are proportional to the corresponding final state DOS weighted by the transition matrix elements, we can make conclusions on the shape of the pDOS based on the experimental spectra measured at low q. The p_{xy} states are concentrated within a narrow window right above the threshold followed by a roughly 5 eV gap before the density starts to increase again. The p_z states are, on the other hand, spread over about 15 eV range with a relatively flat density of states. The s symmetry states have a nearly zero density of states at the threshold as revealed by the q dependence.

These conclusions are further supported by ℓDOS calculated using the MS code. The ℓDOS for the final states and for the ground state are shown in Fig. 3. The Fermi level position, shown by a vertical dashed line in Fig. 3, is at 187.2 eV corresponding roughly to the position of the K-shell threshold in Fig. 1. When comparing the final state densities with the experimental spectra for $\vec{q} \parallel [100]$,

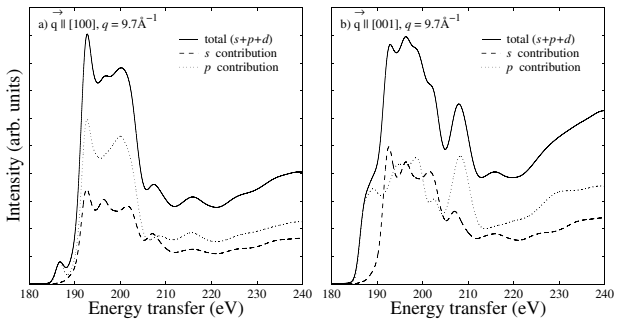

FIG. 2. (a) Decomposition of the boron K-edge XRS spectra calculated using the BSE scheme into contributions from excitations into s and p symmetry final states for $\vec{q} \parallel [100]$ and $q = 9.7$ Å^{-1}. (b) is the same as (a), except $\vec{q} \parallel [001]$.

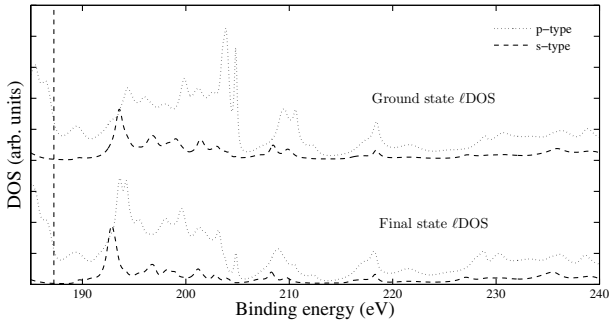

FIG. 3. Multiple scattering calculations of the symmetry projected density of states of boron atoms in MgB_2 for ground state (upper part) and for final state (lower part) of XRS process. The Fermi energy is at 187.2 eV and is shown by a vertical dashed line.

shown in Fig. 1(a), we note that the peak A in the experimental spectra coincides with the peak in pDOS right above the Fermi level, indicating a contribution from p_{xy} type orbitals to this pDOS feature. The broader structure at pDOS around 189 eV underlying the peak right above the Fermi level can be associated with the feature A′ in the $\vec{q} \parallel [001]$ spectra in Fig. 1(b). With very little intensity in the experimental spectra for $\vec{q} \parallel [100]$ around 189 eV energy transfer range, most of the pDOS would be stemming solely from p_z states. Right above the Fermi level the calculation shows almost no states with s symmetry, confirming the earlier conclusion that at the threshold empty states are predominantly of p symmetry.

At higher binding energies the peak in the calculated final state pDOS at 194 eV coincides with the peak B in the $\vec{q} \parallel [100]$ spectra in Fig. 1(a). The shift of the peak B to lower energies by roughly 0.5 eV with increasing q, which was not reproduced in the BSE scheme calculation of the XRS spectra, can be explained by the shape of the sDOS, which has a peaked structure 1 eV below the pDOS peak at 194 eV. With increasing q, contributions from empty s states start to rise and the separation of the two peaks in s and pDOS is seen as a shift of the peak B position in the experimental spectra. Overall, the differences between the final state s and pDOS are in a good agreement with the earlier analysis of the momentum transfer dependence of the spectral features. The above analysis shows how XRS can be used to probe both the spatial orientation and symmetries of the final states and to verify density of states calculations.

In Fig. 1 we showed the MS calculation of the absorption spectra calculated without the core hole in the final state. For $\vec{q} \parallel [100]$ the intensity of the peak A is increased and the intensity of the feature B is reduced considerably. For $\vec{q} \parallel [100]$ a small decrease in the intensity of the feature A′ is observed when compared to a calculation with a core hole. Otherwise the effect of the core hole potential is seen mostly as shifts in the positions of different features into higher energy transfers. These differences are also seen between the ground state and the final state DOS in Fig. 3, where the peak at 195 eV in the pDOS gains intensity in the presence of a core hole. The too large intensity of the peak B in both MS and BSE calculation is probably partly stemming from the overestimation of the attractive part of the core hole potential. Near the Fermi level the core hole potential reduces the p_{xy} and increases the p_z density of states slightly. The overall shape of the sDOS is less affected by the core hole potential, showing mainly shifts in the peak positions. For detailed analysis of spectral features over the whole energy range, the inclusion of the core hole potential is clearly necessary.

In conclusion, we have measured and calculated the XRS spectra at the boron K edge in single crystal MgB_2. Using the momentum transfer dependence of the XRS cross section, our experiment reveals a considerable density of both the p_{xy} (σ band) and p_z (π band) states and a vanishing density of empty s symmetry states near the threshold. These results highlight the crucial role of especially the p_{xy} states in determining the superconducting properties of MgB_2.

This work has been supported by the Academy of Finland (Contracts No. 201291/40732).

*Electronic address: Aleksi.Mattila@helsinki.fi

[1] J. Nagamatsu *et al.*, Nature (London) **410**, 63 (2001).
[2] For an early review, see C. Buzea and T. Yamashita, Supercond. Sci. Technol. **14**, R115 (2001).
[3] S. L. Budko *et al.*, Phys. Rev. Lett. **86**, 1877 (2001).
[4] F. Bouquet *et al.*, Phys. Rev. Lett. **87**, 047001 (2001).
[5] Y. Wang, T. Plackowski, and A. Junod, Physica C (Amsterdam) **355**, 179 (2001).
[6] H. J. Choi *et al.*, Nature (London) **418**, 758 (2002).
[7] H. J. Choi *et al.*, Phys. Rev. B **66**, 020513(R) (2002).
[8] A. Y. Liu, I. I. Mazin, and J. Kortus, Phys. Rev. Lett. **87**, 087005 (2001).
[9] S. Souma *et al.*, Nature (London) **423**, 65 (2003).
[10] J. Kortus *et al.*, Phys. Rev. Lett. **86**, 4656 (2001).
[11] J. M. An and W. E. Pickett, Phys. Rev. Lett. **86**, 4366 (2001).
[12] T. Yildirim *et al.*, Phys. Rev. Lett. **87**, 037001 (2001).
[13] J. S. Slusky *et al.*, Nature (London) **410**, 343 (2001).
[14] Y. Mizuno and Y. Ohmura, J. Phys. Soc. Jpn. **22**, 445 (1967).
[15] Y. Zhu *et al.*, Phys. Rev. Lett. **88**, 247002 (2002).
[16] N. Jiang *et al.*, Phys. Rev. B **66**, 172502 (2002).
[17] R. F. Klie *et al.*, Appl. Phys. Lett. **82**, 4316 (2003).
[18] G. P. Zhang *et al.*, Phys. Rev. B **67**, 174519 (2003).
[19] J. Nakamura *et al.*, Phys. Rev. B **68**, 064515 (2003).
[20] A. P. Hitchcock, J. Electron Spectrosc. Relat. Phenom. **112**, 9 (2000).
[21] T. A. Callcott *et al.*, Phys. Rev. B **64**, 132504 (2001).
[22] H. Nagasawa, S. Mourikis, and W. Schülke, J. Phys. Soc. Jpn. **66**, 3139 (1997).
[23] S. Manninen and K. Hämäläinen, Phys. Rev. B **45**, R3878 (1992).
[24] U. Bergmann, P. Glatzel, and S. P. Cramer, Microchemical Journal **71**, 221 (2002).
[25] C. Sternemann *et al.*, Phys. Rev. B **68**, 035111 (2003).
[26] J. Karpinski *et al.*, Supercond. Sci. Technol. **16**, 221 (2003).
[27] M. E. Jones and R. E. Marsh, J. Am. Chem. Soc. **76**, 1434 (1954).
[28] W. Schülke and H. Nagasawa, Nucl. Instrum. Methods Phys. Res. **222**, 203 (1984).
[29] K. Hämäläinen *et al.*, Phys. Rev. B **54**, 5453 (1996).
[30] E. L. Shirley, Phys. Rev. Lett. **80**, 794 (1998).
[31] J. A. Soininen and E. L. Shirley, Phys. Rev. B **64**, 165112 (2001).
[32] A. L. Ankudinov *et al.*, Phys. Rev. B **58**, 7565 (1998).
[33] For the multiple scattering calculation we used a cluster of radius of 9.1 Å with roughly 330 atoms and the Hedin-Lundqvist self-energy.